

Transcranial direct current stimulation (tDCS) induces adrenergic receptor-dependent microglial morphological changes in mice

<https://doi.org/10.1523/ENEURO.0204-19.2019>

Cite as: eNeuro 2019; 10.1523/ENEURO.0204-19.2019

Received: 29 May 2019

Revised: 5 August 2019

Accepted: 19 August 2019

This Early Release article has been peer-reviewed and accepted, but has not been through the composition and copyediting processes. The final version may differ slightly in style or formatting and will contain links to any extended data.

Alerts: Sign up at www.eneuro.org/alerts to receive customized email alerts when the fully formatted version of this article is published.

Copyright © 2019 Mishima et al.

This is an open-access article distributed under the terms of the Creative Commons Attribution 4.0 International license, which permits unrestricted use, distribution and reproduction in any medium provided that the original work is properly attributed.

1 **1. Manuscript Title**

2 Transcranial direct current stimulation (tDCS) induces adrenergic receptor-dependent
3 microglial morphological changes in mice

4 **2. Abbreviated Title**

5 tDCS-induced microglial changes in mice

6 **3. List all Author Names and Affiliations in order as they would appear in the**
7 **published article**

8 Tsuneko Mishima^{1,*}, Terumi Nagai¹, Kazuko Yahagi¹, Sonam Akther^{1,2,3}, Yuki Oe¹, Hiromu
9 Monai^{1,4}, Shinichi Kohsaka⁵, Hajime Hirase^{1,2,3*}

10

- 11 1. Laboratory for Neuron-Glia Circuitry, RIKEN Center for Brain Science, Wako, Saitama, Japan
12 2. Brain and Body System Science Institute, Saitama University, Saitama, Japan.
13 3. Center for Translational Neuromedicine, Faculty of Health and Medical Sciences, University
14 of Copenhagen, Denmark
15 4. Ochanomizu University, Bunkyo-ku, Tokyo, 112-8610, Japan
16 5. National Institute of Neuroscience, National Center of Neurology and Psychiatry, Kodaira,
17 Tokyo, Japan
18

19 **4. Author Contributions:**

20 TM, KS, and HH designed research. TM, TN, KY, SA, YO, and HM performed research; TM, TN,
21 and KY analyzed data; TM and HH wrote the paper.
22

23 **5. Correspondence should be addressed to (include email address)**

24 Tsuneko Mishima (tsuneko.mishima@riken.jp) or Hajime Hirase (hirase@sund.ku.dk)
25

6. Number of Figures	7	9. Number of words for Abstract	172
7. Number of Tables	0	10. Number of words for Significance Statement	81
8. Number of Multimedia	0	11. Number of words for Introduction	406
		12. Number of words for Discussion	953

26

27 **13. Acknowledgements**

28 We thank the members of the laboratory for comments on the manuscript. We are grateful to
29 the RIKEN CBS-Olympus Collaboration Center for confocal imaging equipment and software.
30 and Dr. Kazuhiro Sohya (NCNP, Japan) for providing transgenic mice.

31 **14. Conflict of Interest**

32 Authors report no conflict of interest.

33

34 **15. Funding sources**

35 This work was supported by RIKEN BSI and CBS, KAKENHI grants (16H01888, 18H05150,
36 18K14859), and HFSP (RGP0036/2014).

37

38 **Abstract**

39 Transcranial direct current stimulation (tDCS) has been reported for its beneficial effects on
40 memory formation and various brain disorders. While the electrophysiological readout of tDCS
41 effects is subtle, astrocytes have been demonstrated to elicit Ca^{2+} elevations during tDCS in a
42 rodent model. This study aimed to elucidate the effects of tDCS on another major glial cell type,
43 microglia, by histology and *in vivo* imaging. tDCS performed in awake conditions induced a
44 significant change in the pixel intensity distribution of Iba-1 immunohistochemistry, and
45 microglial somata were enlarged when examined 3 hr after tDCS. These effects were blocked
46 by adrenergic receptor antagonists or in $\text{IP}_3\text{R}2$ (inositol trisphosphate receptor type 2)-deficient
47 mice, which lack large cytosolic Ca^{2+} elevations in astrocytes. No obvious changes were
48 observed in isoflurane-anesthetized mice. Furthermore, *in vivo* two-photon imaging of microglia
49 showed a reduction of motility that was blocked by a beta-2 adrenergic receptor antagonist. Our
50 observations add support for the influence of noradrenaline in tDCS and suggest possible
51 interactions between microglia and astrocytes to express functional changes associated with
52 tDCS.

53 **Significance Statement**

54 Transcranial direct current stimulation (tDCS) is a neuromodulation procedure in which a weak
55 electric direct current is delivered through the brain for tens of minutes. Despite reported
56 positive effects, the mechanisms of tDCS stimulation are not yet understood well. Here, we
57 examined microglial morphology in the mouse cortex after tDCS. We find that the morphology
58 and morphological dynamics of microglia are altered by tDCS in a manner dependent on
59 adrenergic receptors, supporting the notion that (nor)adrenergic signaling is involved in tDCS.

60

61

62 Introduction

63 Noninvasive neuromodulation is a subject of intense research because of its potential for
 64 treating patients with neuropsychiatric and neurologic conditions. Transcranial direct current
 65 stimulation (tDCS) is the application of a constant and weak electric current to the brain through
 66 the skull. Typical parameters applied in humans are 1 mA over $\sim 30 \text{ cm}^2$ for 10–30 min (Bikson
 67 et al., 2016). A fair body of published literature suggests that tDCS has positive effects on
 68 cognitive abilities and could be an alternative treatment for various brain disorders (Brunoni et
 69 al., 2012; Dedoncker et al., 2016; Fregni and Pascual-Leone, 2007; Nitsche et al., 2009, 2008).
 70 On the other hand, there is a notable degree of skepticism due to mixed outcomes of tDCS
 71 experiments (Horvath et al., 2015a, 2015b; Jalali et al., 2017; Kunzelmann et al., 2018; Medina
 72 and Cason, 2017; Turkakin et al., 2018). The skepticism has been, in part, strengthened by a
 73 recent study that suggested negligible tDCS-induced membrane potential changes in cerebral
 74 cortical neurons (Vöröslakos et al., 2018), implying limited involvement of neuronal discharge
 75 as the prevalent mechanism of tDCS.

76 The circuit and cellular mechanisms for tDCS remain to be understood. Glial cells represent
 77 electrically non-excitable cells in the nervous system. They have been regarded as “support cells”
 78 for the normal function of neurons. Amongst glial cell types, astrocytes and microglia maintain
 79 the extracellular milieu by ion homeostasis and phagocytosis, respectively. Additionally,
 80 astrocytes and microglia have been reported to interact with neuronal synapses (Araque et al.,
 81 2014; Wake et al., 2013). We recently reported that astrocytic Ca^{2+} surges occur during tDCS in
 82 mice. Moreover, tDCS-induced astrocytic Ca^{2+} surges were shown to promote cortical plasticity
 83 and have beneficial effects in a mouse model of depression (Monai et al., 2016; Monai and
 84 Hirase, 2018, 2016). The recruitment of Ca^{2+} activities in astrocytes has prompted us to
 85 investigate another major glial cell type, microglia.

86 Microglia are sensitive to brain tissue damage and transform to reactive microglia upon
 87 inflammation. Iba1 immunohistochemistry (IHC) visualizes the morphology of microglia,
 88 which is profoundly altered in reactive microglia. Following the published observation that
 89 reported the lack of pronounced microglial reactivity after tDCS (Monai et al., 2016), here we
 90 investigated Iba1 IHC in detail by digital image analysis. We report subtle, but significant
 91 effects of tDCS in an awake condition, but not under anesthesia, that depended on adrenergic
 92 receptors. Subsequently, we examined microglial motility by *in vivo* two-photon imaging and
 93 found that tDCS reduces microglial motility.

94 **Materials and Methods**

95 All animal procedures were performed in accordance with the RIKEN animal experimental
96 committee's regulations.

97 **Animals**

98 Adult C57BL/6J and IP₃R2 knockout mice (Futatsugi et al., 2005) were used for
99 immunohistochemical experiments (male, 2–4 months old). BAC-GLT1-G-CaMP7 line 817
100 mice (G7NG817, male, 2–5 months old, RIKEN BRC, resource ID: RBRC09650) were used for
101 transcranial macroscopic imaging of neuronal and astrocytic Ca²⁺ activity (Monai et al., 2016).
102 Iba1-GFP mice (Hirasawa et al., 2005) (male, 3–10 months old) were used for *in vivo*
103 two-photon imaging of microglial morphology.

104 **Surgical procedures**

105 Mice were deeply anaesthetized with isoflurane (1.5–2.0%) and their scalps were exposed by
106 shaving. Each mouse was fixed on a stereotaxic apparatus (Narishige) under isoflurane
107 anesthesia. Throughout the surgery and experiments with anesthetized mice, the body
108 temperature was kept at 37 °C with a heating blanket (BWT-100A, Bio Research Center). After
109 topical application of xylocaine ointment (2% lidocaine) on the scalp, the skull above the
110 sensory cortex was exposed by incision of the scalp and temporal muscle. A custom-made
111 chamber ring was glued to the skull with cyanoacrylate superglue. After the glue settled, we
112 applied dental cement (Fuji LUTE BC, GC Corporation; Super-Bond C&B, Sun Medical) for
113 reinforcement. For two-photon imaging, the inner cavity of the chamber ring was reinforced
114 with additional dental cement to secure the interface for an objective lens. Once the chamber
115 ring was rigidly attached, the mouse was fixed on a custom-made stage via the chamber ring.
116 Thereafter, a small craniotomy ($\phi = 3$ mm, with intact dura) was carefully made using a dental
117 drill.

118 **Habituation to head restraint**

119 The post-surgical recovery period was at least three days for IHC experiments and two weeks
120 for *in vivo* two-photon imaging experiments. Following the recovery period, mice were placed
121 on a water restriction schedule and subjected to an acclimatization procedure for head restraint
122 (Fig. 1B). Food was given *ad libitum*. The acclimatization procedure was performed for seven
123 days.

124 On day 1, each mouse was held in the experimenter's hands and water was given via a syringe
 125 (approximately 0.2 ml). During handling, we let the mouse explore until it entered into a body
 126 tube similar to the one used with the tDCS apparatus. If the mouse entered the body tube, we
 127 repeated the procedure 4–5 times. The total handling time was 10 min for each mouse. From
 128 day 2, the mouse continued to be acclimatized to the experimenter and apparatus with a water
 129 reward (0.1–0.2 ml) for each entry to the body tube. At this point, the mouse's head was quickly
 130 ($< 10\text{--}20$ s) fixed to the apparatus via the chamber ring with its body in the tube. Additional
 131 water and sunflower seeds were provided during head-fixation (10–15 minutes). The total
 132 amount of water given during head-fixation was 1.0 ml/day. In some mice for *in vivo*
 133 two-photon imaging, acclimatization was performed for longer than seven days.

134 **Transcranial DC stimulation.**

135 tDCS was applied on mice under anesthesia (2% isoflurane) or in awake conditions. In either
 136 condition, the anode (stainless wire, $\phi = 350\text{ }\mu\text{m}$) was placed on a sodium chloride-based
 137 conductive gel interface (Z101BA, NIHON-KODEN) spread over a circular area ($\phi = \sim 2\text{ mm}$)
 138 above the primary visual cortex (anterior-posterior -2.9 mm , mediolateral 2.0 mm). The cathode
 139 was connected to the neck skin after topical application of xylocaine ointment. DC (0.1 mA, 10
 140 min) was applied with a custom-made isolated constant-current supply.

141 **Histology**

142 After tDCS application, mice were kept for 30 min or 3 hr before they were sacrificed. After
 143 deep anesthesia by urethane, they were first perfused with 0.9% NaCl and later with fixative
 144 solution (4.0% paraformaldehyde in 0.1 M phosphate buffer, pH 7.4). Following brain removal
 145 and overnight post-fixation in the same fixative, coronal slices ($60\text{ }\mu\text{m}$) were prepared using a
 146 microlicer (PRO 7, Dosaka). For Iba1 staining, sections were incubated in a buffer containing
 147 the primary antibody (1:2000, Wako, 019-19741, Tris-buffered saline with 0.1% Triton X-1000)
 148 overnight. The sections were subsequently washed in phosphate buffered saline and incubated
 149 with the Cy3-conjugated secondary antibody (Invitrogen) for 2 hr for fluorescent labelling. To
 150 evaluate DSP4 efficacy, noradrenergic fibers were labelled by anti-tyrosine hydroxylase (TH)
 151 antibody (1:1000, Millipore, AB152) using sagittal slices ($60\text{ }\mu\text{m}$). For positive control of
 152 microglial reactivity, *E. coli* lipopolysaccharide (LPS, 0.5 mg/kg) was administered by
 153 intraperitoneal (i.p.) injection two days before the mice were sacrificed.

154 **Confocal imaging**

155 Immunolabelled cortical microglia (V2 area) were examined using a confocal microscope
 156 (FV1000, Olympus). Images were acquired with a 60× water immersion objective (UPlanSApo,
 157 NA 1.20) at an excitation wavelength of 559 nm. Imaged areas covered $211.761 \times 211.761 \mu\text{m}^2$
 158 (1024×1024) with an optical sectioning of 0.5 μm . Images were scanned with the one-way
 159 mode (8 μs /pixel exposure).

160 **Drug administration**

161 In some experiments, the following drugs were administered prior to tDCS by i.p. injection:
 162 ICI81551 (TOCRIS, 5 mg/kg bodyweight, 30 min before), Prazosin (Sigma, 10mg/kg, 30 min
 163 before). For ablation of noradrenergic neurons, N-(2-chloroethyl)-N-ethyl-2-bromobenzylamine
 164 (DSP4, Sigma) was injected eleven and seven days prior to tDCS application (50 mg/kg, i.p.
 165 each time). Drugs were dissolved in 0.9% NaCl.

166 ***In vivo* imaging of microglial morphology**

167 Adult Iba1-EGFP transgenic mice (Hirasawa et al., 2005), in which eGFP is expressed
 168 exclusively in microglia, were used to monitor microglial morphological dynamics. All mice
 169 were habituated to the experimental apparatus for more than seven days. On the day of imaging,
 170 the mouse was set on a custom-made stage under a two-photon microscope (B-Scope,
 171 Thorlabs). Microglia located more than 50 μm below the pial surface were imaged under awake
 172 conditions at a wavelength of 920 nm. The laser power was adjusted to ~12 mW at the
 173 preparation (Hines et al., 2009; Pfeiffer et al., 2016; Wake et al., 2009). Depth stacks (24-26
 174 slices, 2 μm Z interval, 512×512 pixels corresponding to $101 \times 101 \mu\text{m}^2$ or $201 \times 201 \mu\text{m}^2$) were
 175 acquired every 60 s.

176 **Analysis**

177 **Iba1 IHC image analysis**

178 Confocal images were used for pixel intensity analysis. Image stacks extending to 15 μm
 179 thickness were collapsed into 2D images by maximum intensity projection. Pixel intensities
 180 were converted to Z scores and the cumulative distribution was computed for each collapsed 2D
 181 image.

182 For soma size analysis, confocal image stacks (45–50 μm thickness) were first filtered with a
 183 $3 \times 3 \times 3$ median filter. The resultant image stacks were collapsed into 2D images by maximum

184 intensity projection. To correct for uneven background, the rolling ball method with a radius of
 185 30 pixels was used for background subtraction. Thereafter, the images were subjected to a 3×3
 186 2D median filter followed by binarization with Yen's thresholding method (ImageJ, NIH) for
 187 soma extraction. In some cases, manual adjustments of threshold were needed. Extracted somata
 188 were approximated to ellipses. Following these automated procedures in ImageJ, extracted
 189 somata were validated by manual inspection. The median of microglial soma size distribution
 190 from each mouse was taken as a data point for statistical comparisons.

191 **TH image analysis**

192 The efficacy of DSP4 was evaluated by calculating the mean intensity of posterior cortical layer
 193 1 tyrosine hydroxylase positive (TH⁺) innervation using ImageJ. Briefly, sagittal brain section
 194 images (60 μm thickness) were acquired by a Keyence microscope (BZ-X710, 0.37 μm pixel
 195 size). Ten to twelve contiguous regions of interest (ROIs, 100×100 μm each) were allocated to
 196 occupy layer 1. A background intensity value was calculated from a neighboring parenchymal
 197 area that does not contain TH⁺ axons. The mean TH⁺ signal intensity of each ROI was
 198 computed as the mean pixel intensity minus the background intensity.

199 **Microglial motility assessment**

200 Quantification of microglial surveillance was performed using custom-written ImageJ and
 201 MATLAB programs (MathWorks). The maximum intensity projection image was computed for
 202 each time point of *xyzt* image stack. The resultant *xyt* image stack was registered for *xy* motion
 203 correction. Next, each slice of the *xyt* stack was processed by the ImageJ 'Subtract Background'
 204 plugin to subtract smooth continuous background with a ball size of 30 pixels. Thereafter,
 205 images were treated with a 2D 3×3 median filter. After this pre-processing, rectangular areas
 206 containing the morphological extent of single microglia were extracted as separate image stacks.
 207 These cell-wise image stacks were then binarized with a single threshold determined by Li's
 208 Minimum Cross Entropy method (ImageJ). Noise reduction was then performed by a cycle of
 209 erosion and dilation. The normalized surveillance area at time *t* was calculated as the number of
 210 pixels that were occupied by the microglia at least once since the beginning of imaging until a
 211 given time *t*, divided by the number of pixels occupied by the microglia at the beginning.
 212 Normalized surveillance area is therefore a monotonically increasing function of time (Fig. 6C,
 213 D for an example). The surveillance index is defined as the ratio of normalized surveillance
 214 areas of a microglia in two different sessions (e.g. control "Before" vs. post-tDCS "After").

215 **Statistical analyses**

216 Statistical analyses were performed using Igor Pro (WaveMetrics). Student's paired t-tests and
 217 Wilcoxon-Mann-Whitney rank-sum tests were used for comparison of two sample populations
 218 with matched data and unmatched data, respectively, unless otherwise noted. Data are expressed
 219 as mean \pm SEM, and P values <0.05 were considered statistically significant. Statistical values
 220 are reported in Table 1.

221 **Results**

222 First, we confirmed tDCS-induced cortex-wide Ca^{2+} elevations (Monai et al., 2016) in the
 223 present setting using G7NG817 transgenic mice that express the G-CaMP7 Ca^{2+} sensor in
 224 astrocytes and a subpopulation of neurons. Mice had been acclimatized to be rigidly fixed to a
 225 head-restraint platform, where tDCS (0.1 mA, 10 min) and transcranial fluorescence imaging
 226 were performed (Fig. 1A and B, see methods). Cortical Ca^{2+} signals elevated immediately after
 227 the passage of the DC current. The peak amplitude of the G-CaMP7 response measured ~ 3 mm
 228 anterior to the anodal position was $39.7 \pm 4.1\%$ (Fig. 1C, N = 4 mice), showing that
 229 tDCS-induced Ca^{2+} elevation is observable with the head chamber-ring configuration. Notably,
 230 tDCS-induced Ca^{2+} elevations were not observed in isoflurane-anesthetized mice (Extended
 231 Data Fig. 1-1). Having demonstrated the effectiveness of tDCS, we used C57BL/6 mice to
 232 investigate microglial morphology after tDCS by Iba1 IHC. Mice were sacrificed either 30 min
 233 or 3 hr after tDCS for perfusion fixation.

234 **Iba1 IHC patterns are affected by tDCS in awake mice**

235 Iba1 IHC visualized highly ramified microglial morphology throughout brain slices of
 236 sham-operated, LPS-treated, and tDCS mice (Fig. 2A, B, I, J). To investigate the impact of
 237 tDCS on the wide-field appearance of Iba1 IHC, we computed the pixel intensity distribution,
 238 which is a proxy of global morphological changes. We analyzed layer 2&3 of the visual cortex
 239 located below the anode, since a previous study demonstrated that tDCS-mediated plasticity
 240 occurs in these layers (Monai et al., 2016). Pixel intensities were converted to Z scores with
 241 which, the cumulative distributions were plotted. We compared head-ring-implanted,
 242 unrestrained control mice (Ctl group) vs. head-ring-implanted, acclimatized,
 243 25-min-head-restrained mice (Sham group) to evaluate possible effects of head restraint. In
 244 Figure 2C, we demonstrate that cumulative pixel intensity distribution is similar between the Ctl
 245 and Sham groups, whereas the pixel intensity distribution shifted significantly in mice with

246 reactive microglia caused by LPS. These results suggest that the head-restraining procedure in
247 acclimatized mice does not cause reactivity in cortical microglia.

248 Next, we compared tDCS and sham-treated mice. The combination of two conditions
249 (isoflurane-anesthetized (Isofl) or awake) and two time points (30 min and 3 hr after tDCS)
250 were investigated (Fig. 2D-G). Pixel intensity distribution was similar between sham and tDCS
251 for isofl-30-min, isofl-3-hr, and awake-30-min experiments; however, the awake-3-hr tDCS
252 data exhibited a visible deviation from the sham group (Fig. 2G). This deviation was caused by
253 a higher proportion of pixels at the high-intensity end. For instance, tDCS had a relatively large
254 presence of pixels that had Z score > 0.6 ($21.2 \pm 1.6\%$ vs $18.2 \pm 1.4\%$, $P=1.7e-5$, t-test).
255 Moreover, a high intensity cluster that has Z score > 2 was apparent in the pixel intensity
256 histogram (Fig. 2H). Consistent with this observation, thresholding with $Z > 2$ preserved more
257 microglial structures in awake-3hr tDCS images than the sham counterpart (Fig. 2I, J). While
258 the cumulative pixel intensity histogram of awake-3hr tDCS deviated in the same direction as
259 LPS, microglial morphology appeared normal with fine ramified processes throughout the
260 extent of the cortex in all tDCS experiments. Thus, tDCS does not appear to cause inflammatory
261 responses.

262 **tDCS enlarges microglial somata in awake mice**

263 While the Z-score-based pixel intensity distribution analysis detected changes in the global
264 appearance of images, it falls short of providing information on specific aspects of
265 morphological alterations. Microglial soma size has been reported to be sensitive to brain
266 environmental changes (Kongsui et al., 2015). Therefore, we measured microglial soma size
267 from Iba1 IHC images (Fig. 3A-C, see methods). First, we compared the median microglial
268 soma size of individual animals (43 cells per mouse on average) for unrestrained control and
269 head-restrained sham groups as we did in Figure 2C. Figure 3D indicates that microglia soma
270 sizes are similar between the control and sham groups (ctl: $45.4 \pm 1.0 \mu\text{m}^2$, 7 mice; sham: $43.4 \pm$
271 $1.0 \mu\text{m}^2$, 7 mice; $P = 0.16^b$, Mann-Whitney Wilcoxon test), suggesting that the microglial soma
272 size of the sham group serves as a valid control for tDCS experiments.

273 Soma size did not differ significantly between the awake-30-min tDCS and sham groups (sham:
274 $41.5 \pm 0.92 \mu\text{m}^2$, 7 mice; tDCS: $41.9 \pm 0.9 \mu\text{m}^2$, 7 mice; Fig. 3E, $P = 1.0^a$). In awake-3-hr
275 experiments, soma size was significantly larger in the tDCS group ($P = 0.017^c$, sham: 43.4 ± 1.0
276 μm^2 , 7 mice; tDCS: $47.5 \pm 1.2 \mu\text{m}^2$, 7 mice; Fig. 3E). On the other hand, soma size did not
277 differ significantly when tDCS was performed on isoflurane-anesthetized mice (3 hr: $P=0.95^f$,

278 Sham: $43.7 \pm 1.8 \mu\text{m}^2$, 6 mice vs. tDCS: $43.2 \pm 1.3 \mu\text{m}^2$, 7 mice; Fig. 3F). These results were
 279 consistent with the pixel intensity distribution analysis (Fig. 2) and suggest that isoflurane
 280 anesthesia hampers tDCS-induced microglial soma enlargement.

281 **tDCS-induced microglial soma enlargement is dependent on adrenergic** 282 **receptors**

283 Recent human and animal studies have implicated the involvement of noradrenaline in tDCS
 284 (Kuo et al., 2017; Monai et al., 2016; Monai and Hirase, 2018; Souza et al., 2018). To examine
 285 the possible contribution of noradrenaline to tDCS-induced microglia soma size, we ablated
 286 noradrenergic cells in the locus coeruleus by the neurotoxin DSP4 (Bekar et al., 2008), which
 287 was confirmed by tyrosine hydroxylase (TH) staining in the sensory cortex (Fig. 4A,B).
 288 Following noradrenergic neuron ablation, we performed tDCS using the awake-3-hr protocol.
 289 As a result, DSP4-treated mice did not show a microglial soma enlargement after tDCS (Fig.
 290 4C, Sham: $47.3 \pm 0.6 \mu\text{m}^2$, 7 mice, tDCS: $44.5 \pm 1.1 \mu\text{m}^2$, 7 mice $P = 0.073^e$).

291 Since astrocytes exhibit profound alpha-1 adrenergic receptor (A1AR)-mediated Ca^{2+} elevations
 292 by tDCS (Monai et al., 2016), astrocytic Ca^{2+} signaling possibly plays a role in the microglial
 293 soma enlargement via an inter-cellular communication. To examine this possibility, we used
 294 $\text{IP}_3\text{R2}$ knockout mice in which Gq GPCR (such as A1AR)-activated intracellular Ca^{2+} elevation
 295 is diminished in astrocytes. Awake-3hr tDCS did not result in significant microglial soma size
 296 changes in $\text{IP}_3\text{R2}$ KO mice ($P=0.73^f$, Sham: $44.6 \pm 1.4 \mu\text{m}^2$, 6 mice, tDCS: $44.4 \pm 0.56 \mu\text{m}^2$, 7
 297 mice, Fig. 5A). We next examined the involvement of A1AR using the specific antagonist
 298 prazosin in wildtype C57BL6/J mice. Similar to $\text{IP}_3\text{R2}$ KO mice, prazosin-treated mice did not
 299 display tDCS-induced microglial soma enlargement compared with the sham control group that
 300 also received the antagonist pretreatment ($P=0.8^g$, sham: $42.6 \pm 0.9 \mu\text{m}^2$, 7 mice, tDCS: $42.3 \pm$
 301 $0.7 \mu\text{m}^2$, 7 mice, Fig. 5B). These results suggest that tDCS-triggered noradrenaline release
 302 affects microglial soma enlargement via A1AR activation and the downstream astrocytic
 303 $\text{IP}_3\text{R2}$ -dependent Ca^{2+} signaling pathway.

304 Furthermore, we asked if activation of beta-adrenergic receptors is also involved. In particular,
 305 microglia are known for high levels of beta-2 adrenergic receptor (B2AR) expression (Tanaka et
 306 al., 2002, Gyoneva and Traynelis, 2013). Accordingly, mice were pretreated with ICI181551, a
 307 selective B2AR blocker, and soma sizes were compared. In the ICI181551 group, tDCS-induced
 308 soma size enlargement was not observed ($P=0.48^h$, Sham: $45.9 \pm 0.8 \mu\text{m}^2$, 6 mice, tDCS: $45.2 \pm$
 309 $1.7 \mu\text{m}^2$, 6 mice, Fig. 5C). These results are indicative of noradrenergic involvement in

310 tDCS-induced microglial changes and suggest that both A1ARs and B2BRs are involved in
 311 tDCS-induced microglial soma enlargement.

312 **tDCS decreases microglial surveillance area *in vivo***

313 One of the striking features of microglia is the motility of their ramified processes. Here, we
 314 directly examined the morphological dynamics of individual microglia in the cortex of awake
 315 mice using a two-photon microscope (Fig. 6A). We used the Iba1-EGFP mouse, in which EGFP
 316 is exclusively expressed in microglia (Hirasawa et al., 2005). We confirmed that microglia
 317 showed surveillance activities by continual extension and retraction of their processes in all
 318 directions (Davalos et al., 2005; Nimmerjahn et al., 2005). For example, overlay of 60-min
 319 imaging resulted in an extensive coverage of the area within ~60 μ m from the soma, while the
 320 soma position remained unmoved (Fig. 6C). We defined normalized surveillance area as the
 321 proportion of cumulative microglia-occupied area at a given time relative to a start time (Fig.
 322 6D). To check if laser scanning has an impact on microglial morphology, we compared the
 323 occupied area of each monitored microglia at the beginnings of “Before” and “After” imaging
 324 sessions of the sham-treated group (Fig. 6E). We found no significant difference, suggesting
 325 that the effect of laser irradiation on microglial morphological dynamics is negligible.

326 While the evolution of normalized surveillance area varied considerably among individual
 327 microglia, the average trace converged to a gradually decelerating curve (Fig. 6F). The mean
 328 surveillance area after 60 minutes did not differ significantly between before and after sham
 329 stimulation. Remarkably, the mean surveillance area index curve of tDCS mice (i.e. “After”
 330 session) is plotted lower than the control condition (i.e. “Before” session). We assessed
 331 individual microglia’s surveillance area change by taking the ratio of surveillance area indices
 332 during “Before” and “After” sessions, demonstrating a significant decrease of surveillance area
 333 by tDCS ($t = 40$ min, $P=0.014^{\dagger}$, paired t-test, Fig. 6G).

334 Furthermore, we addressed if noradrenergic signaling is involved in this tDCS-induced
 335 microglial surveillance reduction by prazosin or ICI181551 pretreatment in awake mice (Fig.
 336 7A). As a reference, we computed the surveillance index comparing “Before” and “After”
 337 sessions at 40 min after the start of respective sessions. As expected from the previous analysis
 338 (Fig. 6G), surveillance index of tDCS experiments was significantly reduced (Fig. 7A).
 339 Prazosin-treated mice showed a similar significant reduction of surveillance index after tDCS
 340 (Fig. 7B). By contrast, ICI181551 treatment abolished tDCS-induced reduction of microglia

surveillance, and a trend for increased surveillance was apparent (Fig. 7C). These results point to a significant role of the B2AR in the inhibition of microglial surveillance activity after tDCS.

Discussion

The present experiments report that tDCS induces subtle, but significant, alterations of Iba1 distribution and microglial motility in the cerebral cortex in awake mice. Furthermore, these alterations were dependent on (nor)adrenergic receptors, which is in line with an earlier study that described tDCS-induced A1AR-dependent astrocytic Ca^{2+} surges (Monai et al., 2016). Notably, while astrocytic Ca^{2+} responses occur during tDCS, morphological alterations of microglia occurred after a few hours.

We demonstrated that microglial soma is enlarged after tDCS. Remarkably, the soma enlargement occurs only in awake mice. It is well established that microglial morphology is radically altered by LPS-induced inflammation (Kondo et al., 2011; Kongsui et al., 2015; Kozłowski et al., 2012). LPS-induced microglial alterations are obvious even with a low dosage of 100 $\mu\text{g/kg}$, whereby approximately 20% soma enlargement has been reported in the prefrontal cortex (Kongsui et al., 2015). The tDCS-induced microglial soma enlargement of a mere several percent in the current study is relatively modest. Moreover, no obvious change was detected in ramified processes. As general anesthesia compromises astrocytic Ca^{2+} activation, in particular noradrenergically driven large-scale and synchronized Ca^{2+} surges (Ding et al., 2013; Thrane et al., 2012), microglial changes by tDCS conceivably depend on the elevated noradrenergic tone during awake states. On the other hand, some studies have reported significant changes in anesthetized mice that underwent tDCS. For instance, one study reported enhancements of GFAP and BDNF in anesthesia changed gene expression (de Souza Nicolau et al., 2018). Another study showed long-lasting anti-depressive behavioral effects (Peanlikhit et al., 2017). However, these studies employed stronger stimulation in terms of stimulus current, duration, and/or frequency. Moreover, the anesthesia condition used in the current study is deeper than the Peanlikhit et al. study. Considering the lack of astrocytic Ca^{2+} surges in this condition (Extended Data Fig. 1-1), our results support the involvement of volume-transmitted neuromodulators in tDCS.

A few studies have examined cortical microglia after tDCS. For instance, Rueger et al. (2012) reported that multi-session tDCS of five to ten days induced a mild sign of microglial activation as observed by an upregulation of Iba1 immunohistochemical signals. The current density

employed in the Rueger et al. study is $\sim 150 \text{ A/m}^2$, whereas that used in the current study is $< 30 \text{ A/m}^2$. Considering the study by Gellner et al. that reported a microglial activation threshold of $30\text{--}50 \text{ A/m}^2$ with light isoflurane anesthesia (Gellner et al., 2016), it is conceivable that our experiments were performed in near-threshold conditions. The tDCS-induced microglial soma enlargement and Iba1 signal intensity distribution shift are different from the microglial morphological alterations reported in a rodent model of electroconvulsive therapy (ECT), in which obvious reductions in process ramification and Iba1 expression occur (Jinno and Kosaka, 2008). The pronounced alterations of microglia by ECT are most likely caused by the high-intensity electric stimulation that induces seizures. By contrast, cortical neuronal discharge activity remains undisturbed by tDCS (Monai et al., 2016; Vöröslakos et al., 2018).

We find that tDCS-induced soma enlargement is dependent on noradrenergic signaling. Moreover, the prazosin and IP₃R2-KO mouse (which lacks astrocytic Ca^{2+} surges) experiments suggest a key mechanism linked to A1AR activation. The previous reports of relative abundance of A1ARs in astrocytes over microglia (Hertz et al., 2010; Zhang et al., 2014) and A1AR-dependent tDCS-induced astrocytic Ca^{2+} surges (Monai et al., 2016) support the idea that astrocytic activation exerts effects on microglia. While this is intriguing, neither the prazosin nor the IP₃R2 KO mouse experiment is cell-type specific, therefore it is possible that direct noradrenergic activation of microglia causes soma enlargement. Indeed, B2AR inhibition by ICI181551 also disrupted microglial somatic enlargement. Functional and transcriptomic evidence underwrites the enriched expression of B2ARs in microglia (Gyoneva and Traynelis, 2013; Tanaka et al., 2002; Zhang et al., 2014).

By imaging microglial morphology in awake mice, we found that tDCS attenuates microglial motility. This effect was also dependent on B2ARs, but not on A1ARs. The inhibitory effect of microglial B2ARs on motility is consistent with the *in vitro* observation by Gyoneva and Traynelis (Gyoneva and Traynelis, 2013) and recent *in vivo* observations in awake mice (Liu et al., 2019; Stowell et al., 2019). It is tempting to speculate that the brake on microglial surveillance creates an opportunity for relevant synapses to establish an initial stage of synaptic plasticity. Microglia have been demonstrated to be a source for brain-derived neurotrophic factor (BDNF) (Parkhurst et al., 2013), a pivotal neurotrophin for synaptic plasticity and neurogenesis. Interestingly, tDCS upregulates *Bdnf* (de Souza Nicolau et al., 2018), promotes BDNF-dependent synaptic plasticity (Fritsch et al., 2010) and causes epigenetic modification to *Bdnf* genomic regions (Podda et al., 2016). It remains to be shown if BDNF synthesis is promoted by (nor)adrenergic activation as is reported in astrocytes (Jurič et al., 2008). In

405 addition to astrocyte-neuron interactions (Cocco et al., 2018; Monai and Hirase, 2016), our
 406 results advocate for the inclusion of microglia as a functional component of tDCS mechanism
 407 via adrenergic receptor activation.

408 One of the limitations of the current study is the lack of microglia-specific molecular
 409 manipulations. While it remains undetermined whether the microglial changes observed in this
 410 study have causal roles for positive outcomes of tDCS, several groups have consistently
 411 reported inflammation-associated microglial soma enlargement (Chen et al., 2012; Kongsui et
 412 al., 2015; Kozłowski et al., 2012). Brain inflammation activates microglia and leads to the
 413 production of pro-inflammatory molecules such as $\text{TNF}\alpha$, $\text{IL-1}\beta$, IL-6 (Hanisch, 2002). It is
 414 possible that these cytokines are involved in the synaptic plasticity induced by tDCS. For
 415 instance, it has been demonstrated that the glial $\text{TNF}\alpha$ has a pivotal role in the regulation of
 416 homeostatic synaptic plasticity (Stellwagen and Malenka, 2006). Future studies should address
 417 the causal relationship, for instance by microglial B2AR knockout mice combined with tDCS
 418 and behavioral performance.

419

420 References

- 421 Araque A, Carmignoto G, Haydon PG, Oliet SHR, Robitaille R, Volterra A (2014)
 422 Gliotransmitters travel in time and space. *Neuron* 81:728–739.
- 423 Bekar LK, He W, Nedergaard M (2008) Locus coeruleus α -adrenergic-mediated activation of
 424 cortical astrocytes in vivo. *Cereb Cortex* 18:2789–2795.
- 425 Bikson M et al. (2016) Safety of Transcranial Direct Current Stimulation: Evidence Based
 426 Update 2016. *Brain Stimul* 9:641–661.
- 427 Brunoni AR, Nitsche MA, Bolognini N, Bikson M, Wagner T, Merabet L, Edwards DJ,
 428 Valero-Cabre A, Rotenberg A, Pascual-Leone A, Ferrucci R, Priori A, Boggio PS, Fregni
 429 F (2012) Clinical research with transcranial direct current stimulation (tDCS): Challenges
 430 and future directions. *Brain Stimul* 5:175–195.
- 431 Chen Z, Jalabi W, Shpargel KB, Farabaugh KT, Dutta R, Yin X, Kidd GJ, Bergmann CC,
 432 Stohlman SA, Trapp BD (2012) Lipopolysaccharide-induced microglial activation and
 433 neuroprotection against experimental brain injury is independent of hematogenous TLR4.
 434 *J Neurosci* 32:11706–15.
- 435 Cocco S, Podda M V, Grassi C (2018) Role of BDNF Signaling in Memory Enhancement
 436 Induced by Transcranial Direct Current Stimulation. *Front Neurosci* 12.
- 437 Davalos D, Grutzendler J, Yang G, Kim J V, Zuo Y, Jung S, Littman DR, Dustin ML, Gan
 438 W-BB (2005) ATP mediates rapid microglial response to local brain injury in vivo. *Nat*
 439 *Neurosci* 8:752–8.

- 440 de Souza Nicolau E, de Alvarenga KAF, Tenza-Ferrer H, Nogueira MCA, Rezende FD, Nicolau
441 NF, Collodetti M, de Miranda DM, Magno LAV, Romano-Silva MA (2018) Transcranial
442 Direct Current Stimulation (tDCS) in Mice. *J Vis Exp*.
- 443 Dedoncker J, Brunoni AR, Baeken C, Vanderhasselt M-A (2016) A Systematic Review and
444 Meta-Analysis of the Effects of Transcranial Direct Current Stimulation (tDCS) Over the
445 Dorsolateral Prefrontal Cortex in Healthy and Neuropsychiatric Samples: Influence of
446 Stimulation Parameters. *Brain Stimul* 9:501–517.
- 447 Ding F, O'Donnell J, Thrane AS, Zeppenfeld D, Kang H, Xie L, Wang F, Nedergaard M (2013)
448 α 1-Adrenergic receptors mediate coordinated Ca^{2+} signaling of cortical astrocytes in
449 awake, behaving mice. *Cell Calcium* 54:387–394.
- 450 Fregni F, Pascual-Leone A (2007) Technology Insight: noninvasive brain stimulation in
451 neurology—perspectives on the therapeutic potential of rTMS and tDCS. *Nat Clin Pract*
452 *Neurol* 3:383–393.
- 453 Fritsch B, Reis J, Martinowich K, Schambra HM, Ji Y, Cohen LG, Lu B (2010) Direct Current
454 Stimulation Promotes BDNF-Dependent Synaptic Plasticity: Potential Implications for
455 Motor Learning. *Neuron* 66:198–204.
- 456 Futatsugi A, Nakamura T, Yamada MK, Ebisui E, Nakamura K, Uchida K, Kitaguchi T,
457 Takahashi-Iwanaga H, Noda T, Aruga J, Mikoshiba K (2005) IP3 receptor types 2 and 3
458 mediate exocrine secretion underlying energy metabolism. *Science* 309:2232–4.
- 459 Gellner A-K, Reis J, Fritsch B (2016) Glia: A Neglected Player in Non-invasive Direct Current
460 Brain Stimulation. *Front Cell Neurosci* 10:188.
- 461 Gyoneva S, Traynelis SF (2013) Norepinephrine modulates the motility of resting and activated
462 microglia via different adrenergic receptors. *J Biol Chem* 288:15291–15302.
- 463 Hanisch UK (2002) Microglia as a source and target of cytokines. *Glia* 40:140–155.
- 464 Hertz L, Lovatt D, Goldman SA, Nedergaard M (2010) Adrenoceptors in brain: cellular gene
465 expression and effects on astrocytic metabolism and $[Ca^{2+}]_i$. *Neurochem Int* 57:411–
466 420.
- 467 Hines DJ, Hines RM, Mulligan SJ, Macvicar BA (2009) Microglia processes block the spread
468 of damage in the brain and require functional chloride channels. *Glia* 57:1610–1618.
- 469 Hirasawa T, Ohsawa K, Imai Y, Ondo Y, Akazawa C, Uchino S, Kohsaka S (2005)
470 Visualization of microglia in living tissues using Iba1-EGFP transgenic mice. *J Neurosci*
471 *Res* 81:357–362.
- 472 Horvath JC, Forte JD, Carter O (2015a) Evidence that transcranial direct current stimulation
473 (tDCS) generates little-to-no reliable neurophysiologic effect beyond MEP amplitude
474 modulation in healthy human subjects: A systematic review. *Neuropsychologia* 66:213–
475 236.
- 476 Horvath JC, Forte JD, Carter O (2015b) Quantitative Review Finds No Evidence of Cognitive
477 Effects in Healthy Populations From Single-session Transcranial Direct Current
478 Stimulation (tDCS). *Brain Stimul* 8:535–550.
- 479 Jalali R, Miall RC, Galea JM (2017) No consistent effect of cerebellar transcranial direct current
480 stimulation on visuomotor adaptation. *J Neurophysiol* 118:655–665.
- 481 Jinno S, Kosaka T (2008) Reduction of Iba1-expressing microglial process density in the
482 hippocampus following electroconvulsive shock. *Exp Neurol* 212:440–447.

- 483 Jurič DM, Lončar D, Čarman-Kržan M (2008) Noradrenergic stimulation of BDNF synthesis in
484 astrocytes: Mediation via $\alpha 1$ - and $\beta 1/\beta 2$ -adrenergic receptors. *Neurochem Int* 52:297–306.
- 485 Kondo S, Kohsaka S, Okabe S (2011) Long-term changes of spine dynamics and microglia after
486 transient peripheral immune response triggered by LPS in vivo. *Mol Brain* 4:27.
- 487 Kongsui R, Johnson SJJ, Graham BAA, Nilsson M, Walker FRR (2015) A combined
488 cumulative threshold spectra and digital reconstruction analysis reveal structural
489 alterations of microglia within the prefrontal cortex following low-dose LPS
490 administration. *Neuroscience* 310:629–640.
- 491 Kozłowski C et al. (2012) An Automated Method to Quantify Microglia Morphology and
492 Application to Monitor Activation State Longitudinally In Vivo. *PLoS One* 7:e31814.
- 493 Kunzelmann K, Meier L, Grieder M, Morishima Y, Dierks T (2018) No Effect of Transcranial
494 Direct Current Stimulation of the Auditory Cortex on Auditory-Evoked Potentials. *Front*
495 *Neurosci* 12:880.
- 496 Kuo H-I, Paulus W, Batsikadze G, Jamil A, Kuo M-F, Nitsche MA (2017) Acute and chronic
497 effects of noradrenergic enhancement on transcranial direct current stimulation-induced
498 neuroplasticity in humans. *J Physiol* 595:1305–1314.
- 499 Liu Y, Li Y, Eyo UB, Chen T, Umpierre A, Zhu J, Bosco DB, Dong H, Wu L-J (2019)
500 Neuronal network activity controls microglial process surveillance in awake mice via
501 norepinephrine signaling. *bioRxiv* 557686.
- 502 Medina J, Cason S (2017) No evidential value in samples of transcranial direct current
503 stimulation (tDCS) studies of cognition and working memory in healthy populations.
504 *Cortex* 94:131–141.
- 505 Monai H, Hirase H (2018) Astrocytes as a target of transcranial direct current stimulation
506 (tDCS) to treat depression. *Neurosci Res* 126:15–21.
- 507 Monai H, Hirase H (2016) Astrocytic calcium activation in a mouse model of tDCS—Extended
508 discussion. *Neurogenesis* 3:e1240055.
- 509 Monai H, Ohkura M, Tanaka M, Oe Y, Konno A, Hirai H, Mikoshiba K, Itohara S, Nakai J,
510 Iwai Y, Hirase H (2016) Calcium imaging reveals glial involvement in transcranial direct
511 current stimulation-induced plasticity in mouse brain. *Nat Commun* 7:11100.
- 512 Nimmerjahn A, Kirchhoff F, Helmchen F (2005) Resting microglial cells are highly dynamic
513 surveillants of brain parenchyma in vivo. *Science* 308:1314–1318.
- 514 Nitsche MA, Boggio PS, Fregni F, Pascual-Leone A (2009) Treatment of depression with
515 transcranial direct current stimulation (tDCS): a review. *Exp Neurol* 219:14–19.
- 516 Nitsche MA, Cohen LG, Wassermann EM, Priori A, Lang N, Antal A, Paulus W, Hummel F,
517 Boggio PS, Fregni F, Pascual-Leone A (2008) Transcranial direct current stimulation:
518 State of the art 2008. *Brain Stimul* 1:206–223.
- 519 Parkhurst CN, Yang G, Ninan I, Savas JN, Yates JR, Lafaille JJ, Hempstead BL, Littman DR,
520 Gan W-B (2013) Microglia promote learning-dependent synapse formation through
521 brain-derived neurotrophic factor. *Cell* 155:1596–1609.
- 522 Peanlikhit T, Van Waes V, Pedron S, Risold P-Y, Haffen E, Etiévant A, Monnin J (2017) The
523 antidepressant-like effect of tDCS in mice: A behavioral and neurobiological
524 characterization. *Brain Stimul*.

- 525 Pfeiffer T, Avignone E, Nägerl UV (2016) Induction of hippocampal long-term potentiation
526 increases the morphological dynamics of microglial processes and prolongs their contacts
527 with dendritic spines. *Sci Rep* 6.
- 528 Podda MV, Cocco S, Mastrodonato A, Fusco S, Leone L, Barbati SA, Colussi C, Ripoli C,
529 Grassi C (2016) Anodal transcranial direct current stimulation boosts synaptic plasticity
530 and memory in mice via epigenetic regulation of Bdnf expression. *Sci Rep* 6:22180.
- 531 Rueger MA, Keuters MH, Walberer M, Braun R, Klein R, Sparing R, Fink GR, Graf R,
532 Schroeter M (2012) Multi-session transcranial direct current stimulation (tDCS) elicits
533 inflammatory and regenerative processes in the rat brain. *PLoS One* 7:e43776.
- 534 Souza A, Martins DF, Medeiros LF, Nucci-Martins C, Martins TC, Siteneski A, Caumo W, dos
535 Santos ARS, Torres ILS (2018) Neurobiological mechanisms of antiallodynic effect of
536 transcranial direct current stimulation (tDCS) in a mice model of neuropathic pain. *Brain*
537 *Res* 1682:14–23.
- 538 Stellwagen D, Malenka RC (2006) Synaptic scaling mediated by glial TNF- α . *Nature*
539 440:1054–1059.
- 540 Stowell RD, Grayson O. S, Ryan P. D, Hanna N B, A. K, Lordy, Jean M. B, Edward B,
541 Mriganka S, Ania K. M (2019) Noradrenergic signaling in wakeful states inhibits
542 microglial surveillance and synaptic plasticity in the mouse visual cortex. *bioRxiv*.
- 543 Tanaka KF, Kashima H, Suzuki H, Ono K, Sawada M (2002) Existence of functional beta1- and
544 beta2-adrenergic receptors on microglia. *J Neurosci Res* 70:232–237.
- 545 Thrane AS, Thrane VR, Zeppenfeld D, Lou N, Xu Q, Nagelhus EA, Nedergaard M, Rangroo
546 Thrane V (2012) General anesthesia selectively disrupts astrocyte calcium signaling in the
547 awake mouse cortex. *Proc Natl Acad Sci U S A* 109:18974–18979.
- 548 Turkakin E, Akbiyık S, Akyol B, GÜrdere C, Çakmak YÖ, Balci F (2018) Differential Bilateral
549 Primary Motor Cortex tDCS Fails to Modulate Choice Bias and Readiness in Perceptual
550 Decision Making. *Front Neurosci* 12:410.
- 551 Vöröslakos M, Takeuchi Y, Brinyiczki K, Zombori T, Oliva A, Fernández-Ruiz A, Kozák G,
552 Kincses ZT, Iványi B, Buzsáki G, Berényi A (2018) Direct effects of transcranial electric
553 stimulation on brain circuits in rats and humans. *Nat Commun* 9:483.
- 554 Wake H, Moorhouse AJ, Jinno S, Kohsaka S, Nabekura J (2009) Resting microglia directly
555 monitor the functional state of synapses in vivo and determine the fate of ischemic
556 terminals. *J Neurosci* 29:3974–80.
- 557 Wake H, Moorhouse AJ, Miyamoto A, Nabekura J (2013) Microglia: actively surveying and
558 shaping neuronal circuit structure and function. *Trends Neurosci* 36:209–217.
- 559 Zhang Y, Chen K, Sloan SA, Bennett ML, Scholze AR, O’Keeffe S, Phatnani HP, Guarnieri P,
560 Caneda C, Ruderisch N, Deng S, Liddelow SA, Zhang C, Daneman R, Maniatis T, Barres
561 BA, Wu JQ (2014) An RNA-Sequencing Transcriptome and Splicing Database of Glia,
562 Neurons, and Vascular Cells of the Cerebral Cortex. *J Neurosci* 34:11929–11947.

563

564 **Figure Legends**

565 **Figure 1**

566 Head-restraint tDCS experiment. A. Experimental setup for tDCS. B. Experimental schedule of
567 immunohistochemical experiment. C. Top view of a BAC-GLT1-G7 Line 817 (G7NG817)
568 mouse. Fluorescent Ca^{2+} signal is transcranially observable. Signals ~ 3 mm anterior to the
569 anodal site ($1 \times 1 \text{ mm}^2$ red square) are plotted from four mice (right, upper traces). The bold trace
570 on the bottom is the mean of the four traces, and the shaded areas represent standard error. The
571 red arrowhead and line indicate the onset of tDCS. Scale bar: 1 mm

573 **Figure 2**

574 Intensity analysis of microglial confocal images. A&B. Representative images of Cy3-labelled
575 Iba1 IHC by maximum intensity projection obtained in sham and LPS-treated mice. Yellow
576 scale bar: $100 \mu\text{m}$ (in A left) and $20 \mu\text{m}$ (in A right and B), respectively. C. Cumulative pixel
577 intensity distribution from unrestrained control (Ctl) and head-restrained, sham-stimulated
578 (Sham) groups were similar and distinct from the LPS-treated group. D-G. Intensity was
579 compared between tDCS- and sham-treated groups under the isoflurane-anesthetized (D, E) or
580 awake (F,G) conditions, perfused at 30 min or 3 hr after sham/tDCS. (H) In awake mice, the
581 pixel intensity histogram indicates that there is a cluster at Z score > 2 (i.e. mean + 2SD) region
582 in the tDCS group (dotted red square). I & J. Representative images from a sham-treated mouse
583 and a tDCS-treated mouse. Images in the red squares correspond to the thresholded images on
584 the left at mean + 2SD. Red scale bars: $20 \mu\text{m}$. ** $P < 0.01$, *** $P < 0.001$

586 **Figure 3**

587 Quantification and comparison of microglial soma size. A. Example image of an Iba1 IHC
588 confocal image stack collapsed by maximum intensity projection. Scale bar: $20 \mu\text{m}$. B. Digitally
589 processed image of A for soma extraction. C. Example of the elliptic approximation of soma
590 (red dotted square in A and B). D. Comparison of median values of microglial soma areas
591 between sham-stimulated and unrestrained control mice ($P = 0.1^a$ Mann-Whitney Wilcoxon
592 rank-sum test). Scale bar: $20 \mu\text{m}$ in A and B, $10 \mu\text{m}$ in C. E. Comparison of microglial soma
593 size in awake mice with/without tDCS-treatment at different time point (30 min or 3 hr) after

594 tDCS. Microglial soma size was larger in the tDCS group in awake-3hr experiment ($P = 0.017^e$,
595 Mann-Whitney Wilcoxon rank-sum test). Each group contains seven mice. F. Microglial soma
596 size comparison in isoflurane-anesthetized mice (Isofl-3hr)

597

598 **Figure 4**

599 tDCS-induced microglial somatic enlargement depends on noradrenaline.

600 A. Example of cortical image (inverted grayscale) from saline (left) or DSP4 (right) pretreated
601 mice stained with TH-antibody. B. Mean intensity analysis of TH+ fiber. Each group contains
602 data from three mice. Data from the same animals are plotted with the same symbol and color.
603 Scale bars: 100 μm . C. Comparison between median glial soma size from sham- and
604 tDCS-treated mice (Sham: 7 mice, tDCS: 7 mice, $P = 0.073^e$, Mann-Whitney Wilcoxon
605 rank-sum test)

606

607 **Figure 5**

608 tDCS-induced microglial somatic enlargement depends on B2AR and A1AR pathways. A.
609 Comparison between median microglial soma size between sham- and tDCS-treated IP₃R2 KO
610 mice (Sham: 6 mice, tDCS: 7 mice, $P = 0.73^f$).

611 B&C. Comparison of microglial soma size between sham and tDCS-treated wild-type strain
612 C57BL/6/J with prazosin (B, Sham: 7 mice, tDCS: 7 mice, $P = 0.8^g$), or ICI181551 pretreatment
613 (C, Sham: 6 mice, tDCS: 6 mice, $P = 0.48^h$).

614

615 **Figure 6**

616 *In vivo* monitoring of microglial morphological dynamics.

617 Experimental set up (A) and time schedule of *in vivo* two-photon imaging (B). C.
618 Representative images of a microglia overlaid from $t = 0$ to respective time points (10, 30, 40
619 min). D. Normalized surveillance area curve during 60-min imaging period. Red arrowheads
620 show the time points for the images in C. Scale bar: 10 μm .

621 E. Initial microglial area at $t = 0$ of “Before” and “After” sessions are similar in sham mice (13
622 cells from 8 mice, $P=0.82^i$) Blue lines represent data from individual microglia and the black
623 line represents averaged data.

624 F. Normalized surveillance area curves during the 60-min imaging period before (blue) and after
625 (red) stimulation in the sham (left) and tDCS (right) mice. Data are represented as mean \pm SEM.

626 G. Normalized surveillance area at $t = 40$ min in “Before” and “After” sessions in tDCS-treated
627 mice (normalized by surveillance area at $t=0$ /before). Red lines represent data from individual
628 microglia and the black line represents averaged data. $P = 0.014^j$, paired t-test.

629

630 **Figure 7**

631 Microglial surveillance is compromised by tDCS. A. Surveillance index at $t = 40$ min after
632 sham/tDCS treatment in no drug-treated animals (sham: 13 cells from 8 mice, tDCS: 11 cells
633 from 8 mice, $P = 0.006^k$) B. Surveillance index comparison in prazosin pretreated mice (sham: 9
634 cells from 2 mice, tDCS: 11 cells from 3 mice, $P = 0.015^l$). C. Surveillance index comparison in
635 ICI181551 pretreated mice (sham: 9 cells from 3 mice, tDCS: 12 cells from 3 mice, $P=0.023^m$)
636 Mann-Whitney Wilcoxon rank-sum test.

637

638 **Extended Data Figure 1-1**

639 Cortical Ca^{2+} activity during tDCS in mice under deep isoflurane anesthesia. G-CaMP7 signal
640 was transcranially measured from isoflurane-anesthetized (1.5–2.0%) BAC-GLT1-G7 Line 817
641 (G7NG817) mice. The upper trace is for sham stimulation ($-3.14 \pm 0.02\%$) and the lower trace
642 is for tDCS (0.1 mA, 10 min, $-4.30 \pm 0.02\%$). Bold traces represent the mean traces of 11 traces
643 from 9 mice. Shaded areas represent standard error. The red arrowhead and vertical line indicate
644 the onset of tDCS or sham stimulation.

Table 1. Statistical Table

	Sample number: cells(animals)	Test type	p-value	Power
a	Sham:334(7), Ctl:315(7)	Mann-Whitney Wilcoxon rank-sum test	0.1	
b	Sham:315(7), tDCS:314(7)	Mann-Whitney Wilcoxon rank-sum test	0.16	
c	Sham:309(7), tDCS:301(7)	Mann-Whitney Wilcoxon rank-sum test	**0.017	
d	Sham:278(6), tDCS:296(7)	Mann-Whitney Wilcoxon rank-sum test	0.95	
e	Sham:285(7), tDCS:319(7)	Mann-Whitney Wilcoxon rank-sum test	0.073	
f	Sham:238(6), tDCS:356(7)	Mann-Whitney Wilcoxon rank-sum test	0.73	
g	Sham:274(7), tDCS:310(7)	Mann-Whitney Wilcoxon rank-sum test	0.8	
h	Sham:266(6), tDCS:282(6)	Mann-Whitney Wilcoxon rank-sum test	0.48	
i	Sham:13(8)	paired t-test	0.82	0.055
j	tDCS:11(8)	paired t-test	**0.014	0.77
k	Sham:13(8), tDCS:11(8)	Mann-Whitney Wilcoxon rank-sum test	***0.006	
l	Sham:11(3), tDCS:9(2)	Mann-Whitney Wilcoxon rank-sum test	**0.015	
m	Sham:9(3), tDCS:12(3)	Mann-Whitney Wilcoxon rank-sum test	**0.023	

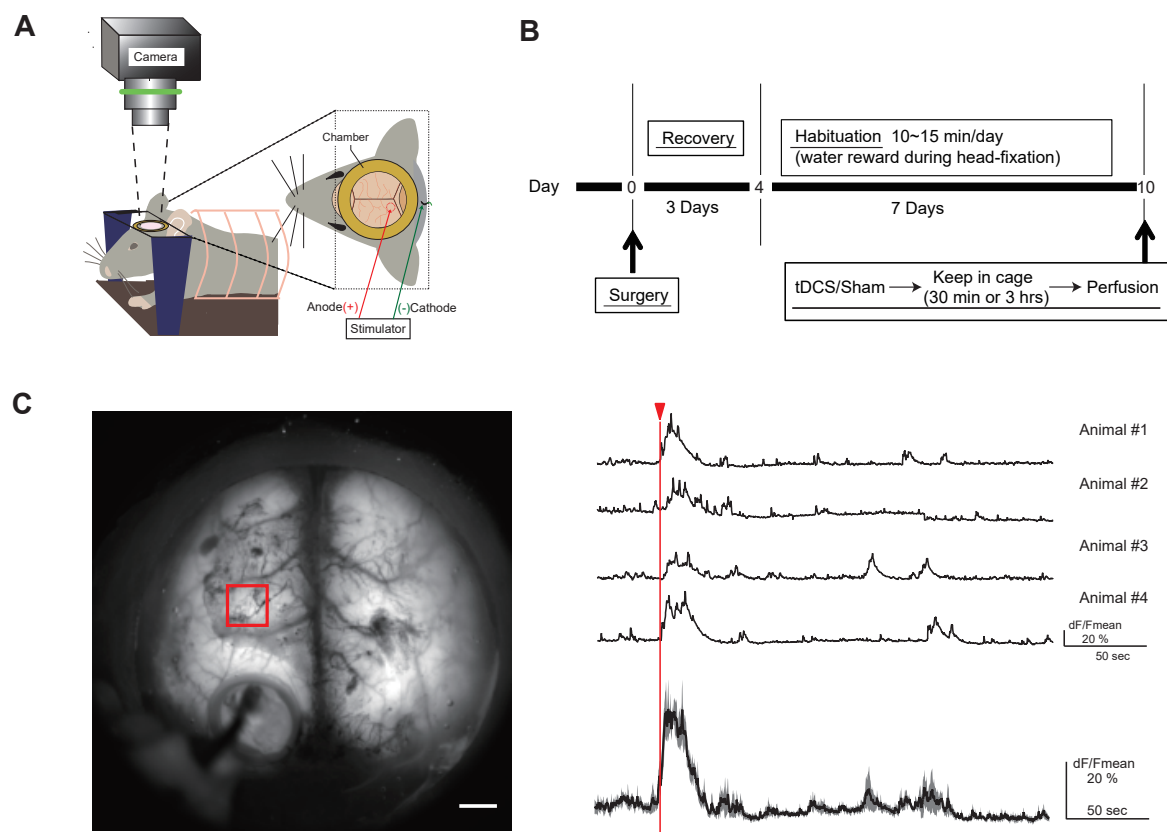


Figure 1

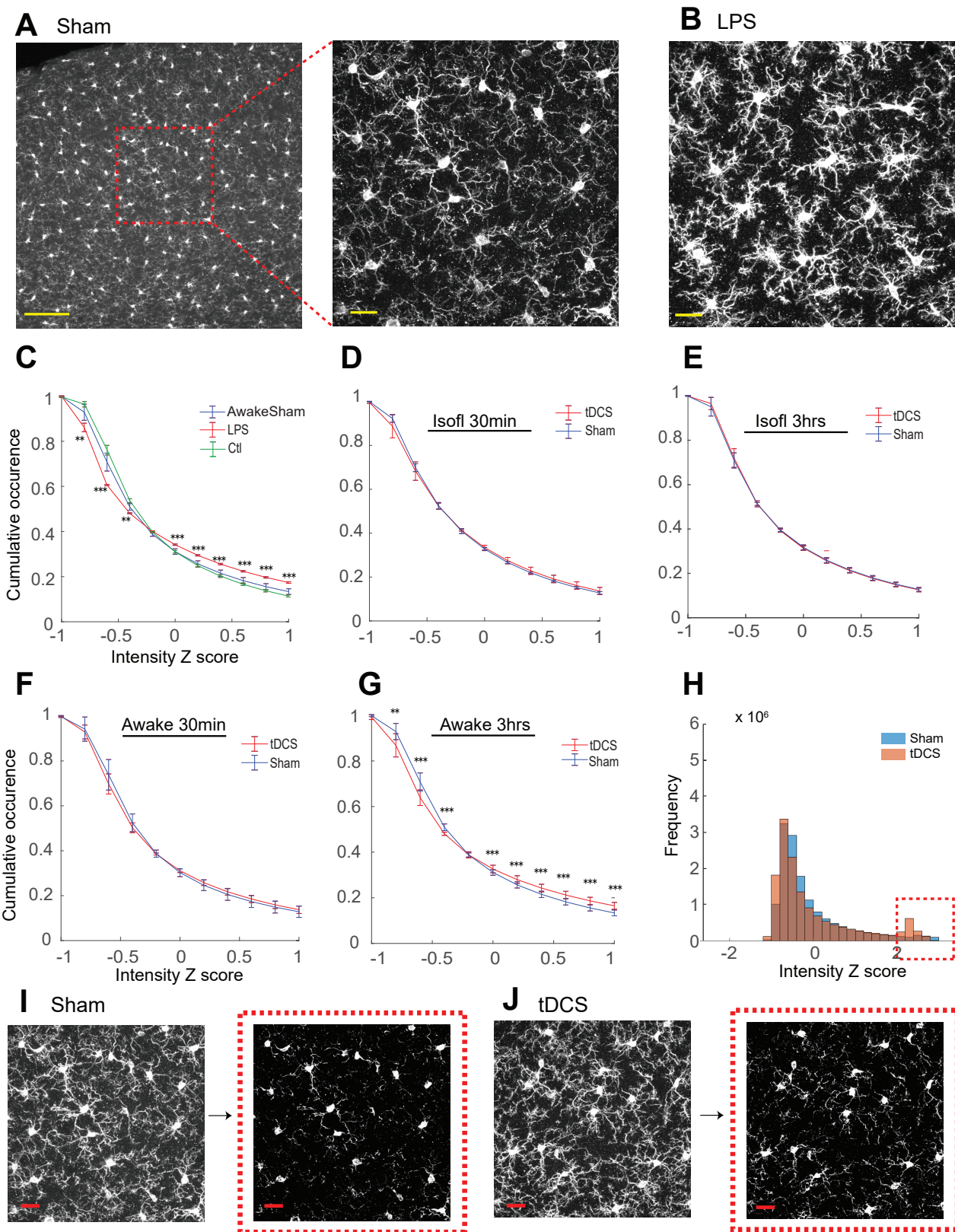


Figure 2

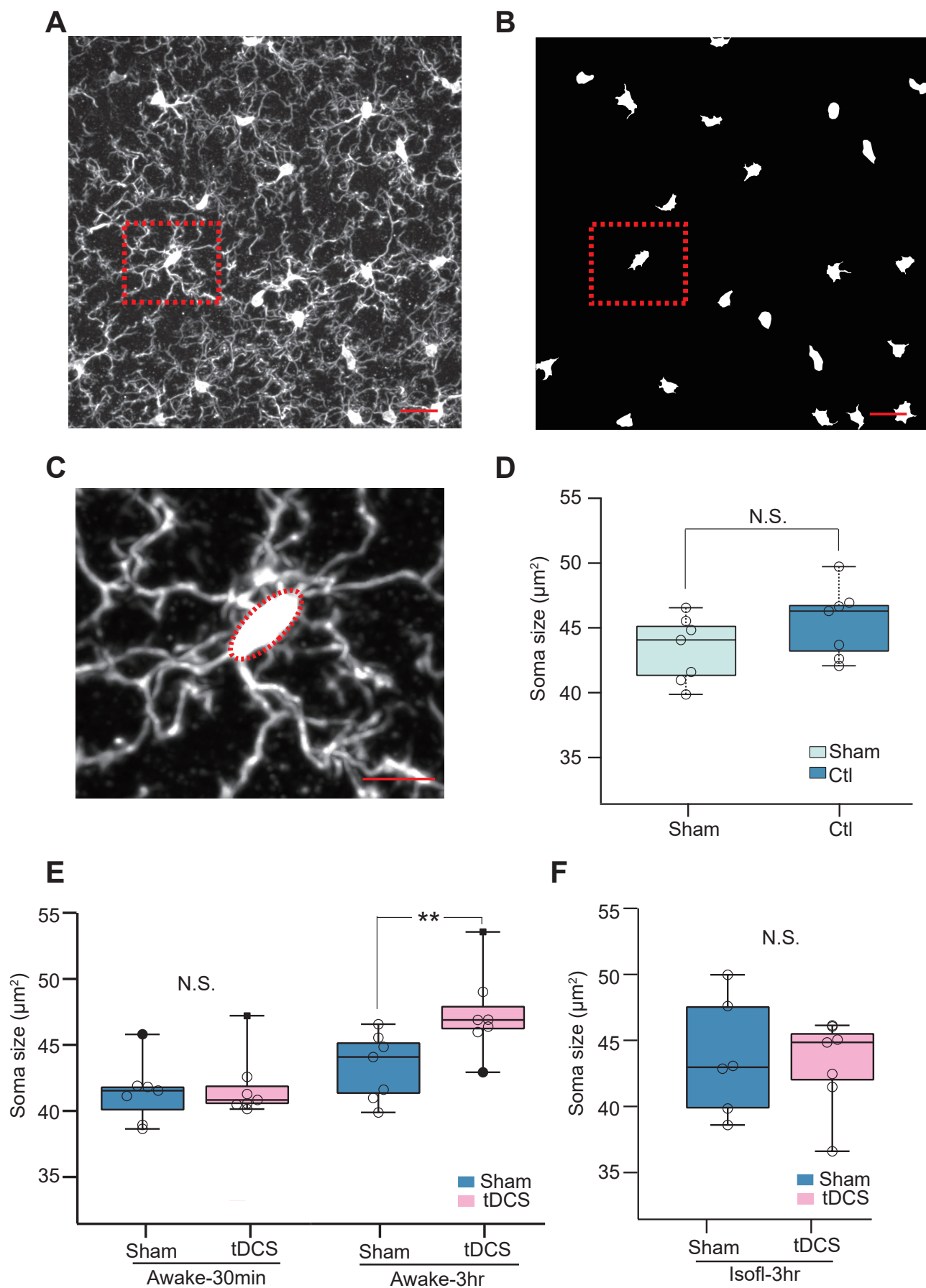


Figure 3

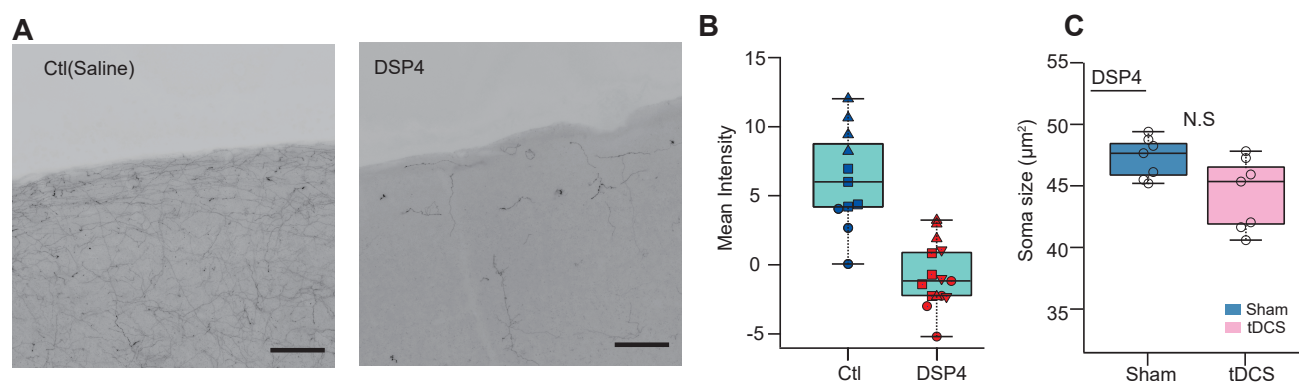


Figure 4

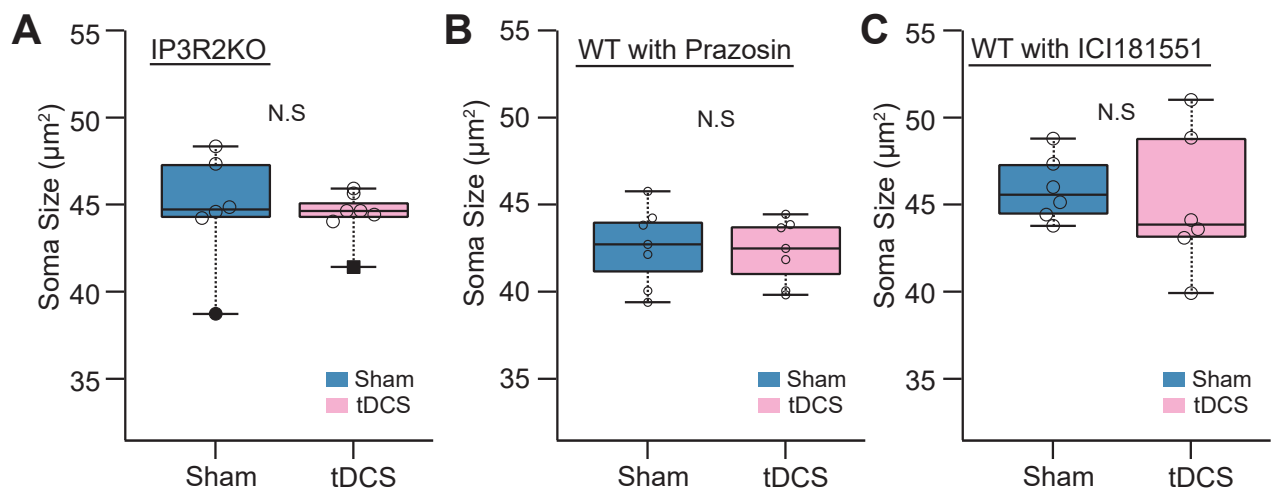


Figure 5

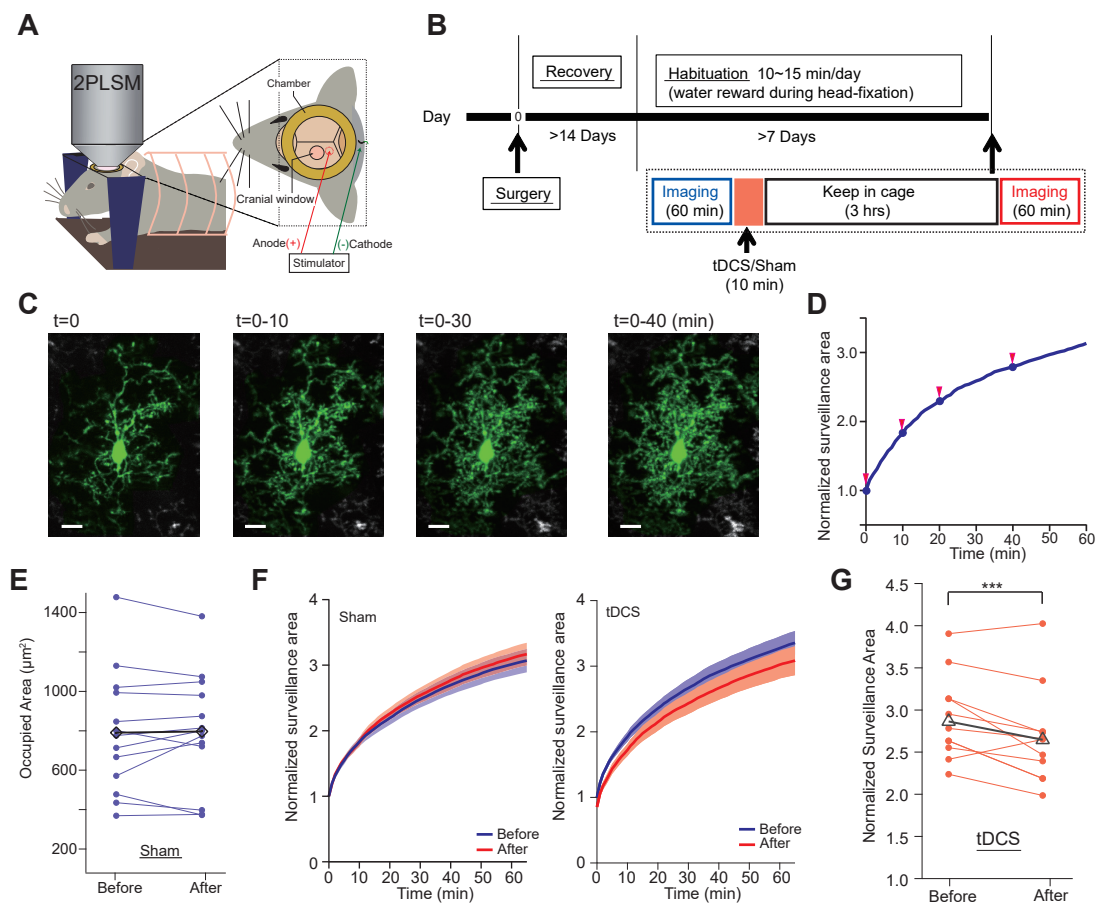


Figure 6

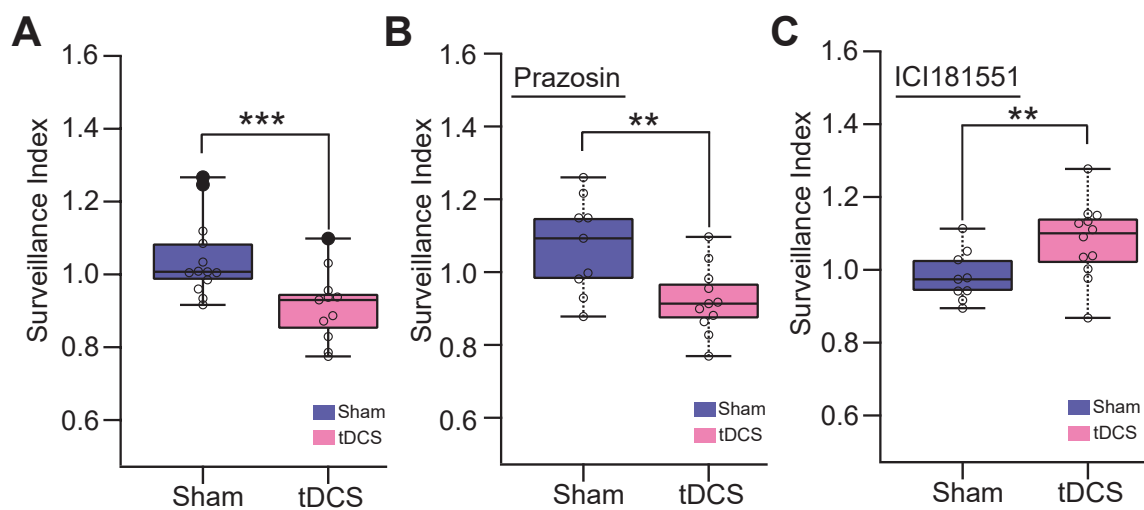


Figure 7